

# Manipulating Highly Deformable Materials Using a Visual Feedback Dictionary

Biao Jia, Zhe Hu, Jia Pan, Dinesh Manocha

**Abstract**—The complex physical properties of highly deformable materials like clothes pose significant challenges for autonomous robotic manipulation systems. We present a novel visual feedback dictionary-based method <sup>1</sup> for manipulating deformable objects towards a desired configuration. Our approach is based on visual servoing and we use an efficient technique to extract key features from the RGB sensor stream in the form of histogram of deformable model features. These histogram features serve as high-level representations of the state of the deformable material. Next, we collect manipulation data and use a visual feedback dictionary that maps the velocity in the high-dimensional feature space to the velocity of the robotic end-effectors for manipulation. We have evaluated our approach on a set of complex manipulation tasks as well as human-robot manipulation tasks on different cloth pieces with varying material characteristics.

## I. INTRODUCTION

The problem of manipulating highly deformable materials such as clothes and fabrics frequently arises in different applications. These include laundry folding [1], robot-assisted dressing or household chores [2], [3], ironing [4], coat checking [5], sewing [6], and transporting large materials like cloth, leather, and composite materials [7]. Robot manipulation has been extensively studied for decades and there is extensive work on the manipulation of rigid and deformable objects. Compared to the manipulation of a rigid object, whose state can be completely described by a six-dimensional configuration space, the manipulation of a deformable object is more challenging due to its very high configuration space dimensionality. The resulting manipulation algorithm needs to handle this dimensional complexity and maintain the tension to perform the task.

Many techniques have been proposed for the automated manipulation of flexible materials. Some of them have been designed for specific tasks, such as peg-in-hole and laying down tasks with small elastic parts [8] or wrapping a cloth around a rigid surface [9]. There is extensive work on folding laundry using pre-planned materials. One practical approach to dealing with general deformable object manipulation is based on visual servoing, [10], [11]. At a broad level, these servoing techniques use the perception data captured using cameras and formulate a control policy mapping to compute the velocities of the robotic end-effectors in realtime. However, a key issue in these methods is to automatically extract key low-dimensional features of the deformable material that can be used to compute a mapping. The simplest methods use manual or other techniques to extract features corresponding to line segments or curvature from a set

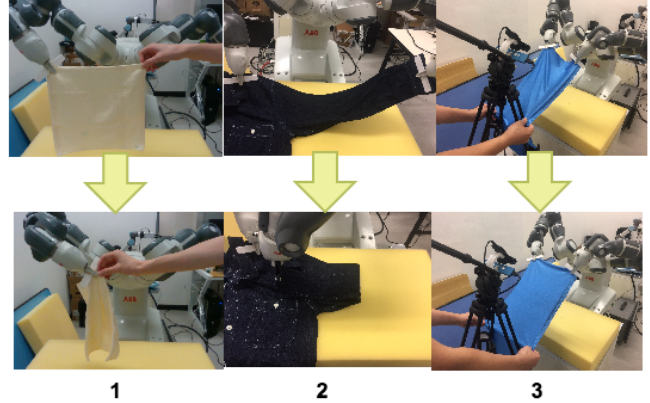


Fig. 1. **Manipulation Benchmarks:** We highlight the realtime performance of our algorithm on three tasks: (1) human-robot jointly folding a cloth with one hand each; (2) robot folding a cloth with two hands; (3) human-robot stretching a cloth with four combined hands. The top row shows the initial state for each task and the bottom row is the final state. Our approach can handle the perturbations due to human movements.

of points on the surface of the deformable material. In addition, we need appropriate mapping algorithms based on appropriate low-dimensional features. Current methods may not work well while performing complex tasks or when the model undergoes large deformations. Furthermore, in many human-robot systems, the deformable material may undergo unknown perturbations and it is important to design robust manipulation strategies [3], [12].

**Main Results:** In this paper, we present a novel feature representation, a histogram of oriented wrinkles (HOW), to describe the shape variation of a highly deformable object like clothing. These features are computed by applying Gabor filters and extracting the high-frequency and low-frequency components. We precompute a visual feedback dictionary using an offline training phase which stores a mapping between these visual features and the velocity of the end-effector. At runtime, we automatically compute the goal configurations based on the manipulation task and use sparse linear representation to compute the velocity of the controller from the dictionary (Section III). Furthermore, we extend our approach so that it can be used in human-robot collaborative settings. Compared to prior manipulation algorithms, the novel components of our work include:

- A novel histogram feature representation of highly deformable materials (HOW-features) that are computed directly from the streaming RGB data using Gabor filters (Section IV).

<sup>1</sup>video is available at [goo.gl/mDSC4H](http://goo.gl/mDSC4H)

- A sparse representation framework using visual feedback dictionary, which directly correlates the histogram features to the control instructions (Section V).
- The combination of deformable feature representation, visual feedback dictionary, and sparse linear representations that enables us to perform complex manipulation tasks, including human-robot collaboration, without significant training data (Section V(C)).

We have integrated our approach with an ABB YuMi dual-arm robot and a camera for image capture and used it to manipulate different cloth materials for different tasks. We highlight the real-time performance for tasks related to stretching, folding, and placement (Section VI).

## II. RELATED WORK

In this section, we give a brief review of prior work on deformable object representation, manipulation, and visual servoing.

### A. Deformable Object Representation

The recognition and detection of deformable object characteristics is essential for manipulation tasks. There is an extensive work in computer vision and related areas on tracking features of deformable models. Some of the earlier work is based on active deformable models [13]. Ramisa *et al.* [14] identify the grasping positions on a cloth with many wrinkles using a bag-of-features-based detector. Li *et al.* [15] encode the category and pose of a deformable object by collecting a large set of training data in the form of depth images from different view points using offline simulation.

### B. Deformable Object Manipulation

Robotic manipulation of general deformable objects relies on a combination of different sensor measurements. The RGB images or RGB-Depth data are widely used for deformable object manipulation [1], [4], [11]. Fiducial markers can also be printed on the deformable object to improve the manipulation performance [16]. Besides visual perception, information from other sensors can also be helpful, like use of contact force sensing to maintain the tension [7]. In many cases, simulation techniques are used for manipulation planning. Clegg *et al.* [17] use reinforcement learning to train a controller for haptics-based manipulation. Bai *et al.* [18] use physically-based optimization to learn a deformable object manipulation policy for a dexterous gripper. These simulation-based approaches need accurate deformation material properties, which can be hard. Data-driven techniques have been used to design the control policies for deformable object manipulation. Yang *et al.* [19] propose an end-to-end framework to learn a control policy using deep learning techniques for folding clothes. Cusumano-Towner *et al.* [20] learn a Hidden Markov Model (HMM) using a sequence of manipulation actions and observations.

$m$	state of the deformable object
$r$	robot's end-effector configuration
$v$	robot's end-effector velocity, $v = \dot{r}$
$I(w, h)$	image from the camera, of size $(w_I, h_I)$
$s(I)$	HOW-feature vector extracted from image $I$
$d_i(I)$	the $i$ -th deformation kernel filter
$I^{(t)}, r^{(t)}$	time index
$\{\Delta s^{(i)}\}, \{\Delta r^{(i)}\}$	features and labels of the visual feedback dictionary
$\rho(\cdot, \cdot)$	error function between two items
$\lambda$	positive feedback gain
$L$	interaction matrix linking velocities of
$F$	the feature space to the end-effector configuration space
$p_j(i)$	interaction function linking velocities of
$N_{dof, I, r, d}$	the feature space to the end-effector configuration space
$C_{fr}$	$j_{th}$ histogram of value $i$
$r^*, s^*, m^*$	number of degrees of freedom of the manipulator, images $\{I^{(t)}\}$ , samples $\{r^{(t)}\}$ , filters $\{d^{(t)}\}$
$\hat{r}, \hat{s}, \hat{m}$	constant of frame rate
	desired target
	approximated target

TABLE I  
SYMBOLS USED IN THE PAPER

### C. Visual Servoing for Deformable Objects

Visual servoing techniques [21], [22] aim at controlling a dynamic system using visual features extracted from images. They have been widely used in robotic tasks like manipulation and navigation. Recent work includes the use of histogram features for rigid objects [23]. Sullivan *et al.* [13] use a visual servoing technique to solve the deformable object manipulation problem using active models. Navarro-Alarcon *et al.* [10], [11] use an adaptive and model-free linear controller to servo-control soft objects, where the object's deformation is modeled using a spring model [24]. Langsfeld *et al.* [25] perform online learning of part deformation models for robot cleaning of compliant objects. Our goal is to extend these visual servoing methods to perform complex tasks on highly deformable materials.

## III. OVERVIEW

In this section, we introduce the notation used in the paper. We also present a formulation of the deformable object manipulation problem. Next, we give a brief background on visual servoing and the feedback dictionary. Finally, we give an overview of our deformable manipulation algorithm that uses a visual feedback dictionary.

### A. Problem Formulation

The goal of manipulating a highly deformable material is to drive a soft object towards a given target state ( $m^*$ ) from its current state ( $m$ ). The state of a deformation object ( $m$ ) can be rather complex due to its very high dimensional configuration. In our formulation, we do not represent it explicitly and treat it as a hidden variable. Instead, we keep track of the deformable object's current state in the feature space ( $s$ ) and its desired state ( $s^*$ ), based on HOW-features. The visual servo-control is performed by computing an appropriate velocity ( $v$ ) of the end-effectors. Given the visual feedback about the deformable object, the control velocity ( $v$ ) reduces the error in the feature space ( $s - s^*$ ). After continuously applying feedback control, the

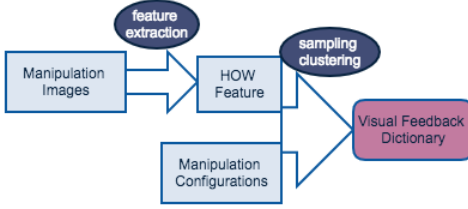


Fig. 2. **Computing the Visual Feedback Dictionary:** The input to this offline process is the recorded manipulation data with images and the corresponding configuration of the robot's end-effector. The output is a visual feedback dictionary, which links the velocity of the features and the controller.

robot will manipulate the deformable object toward its goal configuration. In this way, the feedback controller can be formulated as computing a mapping between the velocity in the feature space of the deformable object and the velocity in the end-effector's configuration space ( $r$ ):

$$r^* - r = -\lambda F(s - s^*) \quad (1)$$

where  $F$  is an interaction function that is used to map the two velocities in different spaces and  $\lambda$  is the feedback gain. This formulation works well only if some standard assumptions related to the characteristics of the deformable object hold. These include infinite flexibility with no energy contribution from bending, no dynamics, and being subject to gravity and downward tendency (see details in [26]). For our tasks of manipulating highly deformable materials like clothes or laundry at a low speed, such assumptions are valid.

### B. Visual Servoing

In this section we give a brief overview of visual servoing [21], [27], [23], [28], which is used in our algorithm. In general-purpose visual servoing, the robot wants to move an object from its original configuration ( $r$ ) towards a desired configuration ( $r^*$ ). In our case, the object's configuration ( $r$ ) also corresponds to the configuration of the robot's end-effector, because the rigid object is fixed relative to the end-effectors during the manipulation task. These methods use a cost function  $\rho(\cdot, \cdot)$  as the error measurement in the image space and the visual servoing problem can be formulated as an optimization problem:

$$\hat{r} = \arg \min_r \rho(r, r^*), \quad (2)$$

where  $\hat{r}$  is the configuration of the end-effector after the optimization step and is the closest possible configuration to the desired position ( $r^*$ ). In the optimal scenario,  $\hat{r} = r^*$ .

Let  $s$  be a set of HOW-features extracted from the image. Depending on the configuration  $r$ , the visual servoing task is equivalent to minimizing the Euclidean distance in the feature space and this can be expressed as:

$$\hat{r} = \arg \min_r ((s(r) - s^*)^T (s(r) - s^*)), \quad (3)$$

where  $s^* = s(r^*)$  is the HOW-feature corresponding to the goal configuration ( $r^*$ ). The visual servoing problem can

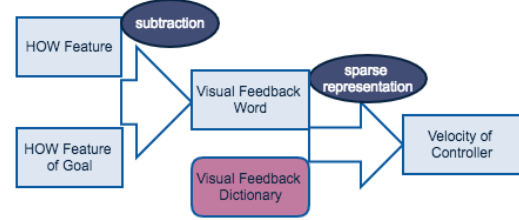


Fig. 3. **Runtime Algorithm:** The runtime computation consists two stages. We extract the deformable features (HOW-features) from the visual input and computes the visual feedback word by subtracting the extracted features from the features of the goal configuration. We apply the sparse representation and compute the velocity of the controller for manipulation.

be solved by iteratively updating the velocity of the end-effectors according to the visual feedback:

$$v = -\lambda L_s^+ (s - s^*), \quad (4)$$

where  $L_s^+$  is the pseudo-inverse of the interaction matrix  $L_s = \frac{\partial s}{\partial r}$ . It corresponds to interaction matrix that links the variation of the velocity in the feature space  $\dot{s}$  to the velocity in the end-effector's configuration space.  $L_s^+$  is computed offline using a non-linear minimization algorithm like Levenberg-Marquardt's algorithm.

### C. Visual Feedback Dictionary

The visual feedback dictionary corresponds to a set of vectors with instances of visual feedback  $\{\Delta s^{(i)}\}$  and the corresponding velocities of the end-effectors  $\{v^{(i)}\}$ , where  $\{\Delta s^{(i)}\} = (s - s^*)$ . Furthermore, we refer to each instance  $\{\Delta s^{(i)}, v^{(i)}\}$  as the *visual feedback word*. This dictionary is computed from the recorded manipulation data. The input includes a set of images ( $\{I^{(t)}\}$ ) and the end-effector configurations ( $\{r^{(t)}\}$ ). Its output is computed as ( $\{\{\Delta s^{(i)}\}, \{v^{(i)}\}\}$ ). We compute this dictionary during an offline learning phase using sampling and clustering methods (see Algorithm 2 for details), and use this dictionary at runtime to compute the velocity of the controller by computing the sparse decomposition of a feedback  $\Delta s$ . More details about computing the visual feedback dictionary are give in Algorithm 2.

### D. Offline and Runtime Computations

Our approach computes the visual dictionary using an offline process (see Fig. 2). Our runtime algorithm consists of two components. Given the camera stream, we extract the HOW-features from the image ( $s(I)$ ) and compute the corresponding velocity of the end-effector using an appropriate mapping. For the controlling procedure, we use the sparse representation method to compute the interaction matrix, as opposed to directly solving the optimization problem (Equation 2). In practice, the sparse representation method is more efficient. The runtime phase performs the actual visual servoing with the current image at time  $t$  ( $I^{(t)}$ ), the visual feedback dictionary ( $\{\{\Delta s^{(i)}\}, \{v^{(i)}\}\}$ ), and the desired goal configurations given by ( $I^*$ ) as the input.

## IV. HISTOGRAM OF DEFORMATION MODEL FEATURE

In this section, we present our algorithm to compute the HOW-features from the camera stream. These are low-dimensional features of the highly deformable material. The pipeline of our HOW-feature computation process is shown in Figure 4. Next, we explain each of these stages in detail.

### A. Foreground Segmentation

In order to find the foreground partition of a cloth, we apply the Gaussian mixture algorithm [29] on the RGB data captured by the camera. The intermediate result of segmentation is shown in Figure 4(2).

### B. Deformation Enhancement

In order to model the high dimensional characteristics of the highly deformable material, we use deformation enhancement. This is based on the perceptual observation that most deformations can be modeled by shadows and shape variations. Therefore, we extract the features corresponding to shadow variations by applying a Gabor transform [30] to the RGB image. This results in the enhancement of the ridges, wrinkles, and edges (see Figure 4). We convolve the  $N$  deformation filters  $\{d_i\}$  to the image  $I$  and represent the result as  $\{d_i(I)\}$ .

In the spatial domain, a 2D Gabor filter is a Gaussian kernel function modulated by a sinusoidal plane wave [31] and it has been used to detect wrinkles [32]. The 2D Gabor filter can be represented as follows:

$$g(x, y; \lambda, \theta, \phi, \sigma, \gamma) = \exp\left(-\frac{x'^2 + \gamma^2 y'^2}{2\sigma^2}\right) \sin\left(2\pi \frac{x'}{\lambda} + \phi\right), \quad (5)$$

where  $x' = x \cos \theta + y \sin \theta$ ,  $y' = -x \sin \theta + y \cos \theta$ ,  $\theta$  is the orientation of the normal to the parallel stripes of the Gabor filter,  $\lambda$  is the wavelength of the sinusoidal factor,  $\phi$  is the phase offset,  $\sigma$  is the standard deviation of the Gaussian, and  $\gamma$  is the spatial aspect ratio. When we apply the Gabor filter to our deformation model image, the choice of wavelength ( $\lambda$ ) and orientation ( $\theta$ ) are the key parameters with respect to the wrinkles of deformable materials. As a result, the deformation model features consist of multiple Gabor filters ( $d_{1\dots n}(I)$ ) with different values of wavelengths ( $\lambda$ ) and orientations ( $\theta$ ).

### C. Grids of Histogram

A histogram-based feature is an approximation of the image which can reduce the data redundancy and extract a high-level representation that is robust to local variations in an image. Histogram-based features have been adopted to achieve a general framework for photometric visual servoing [23]. Although the distribution of the pixel value can be represented by a histogram, it is also significant to represent the position in the feature space of the deformation to achieve the manipulation task. Our approach is inspired by the study of grids of Histogram of Oriented Gradient [33], which is computed on a dense grid of uniformly spatial and orientation cells.

We compute the grids of histogram of deformation model feature by dividing the image into small spatial regions and accumulating local histogram of different filters ( $d_i$ ) of the region. For each grid, we compute the histogram in the region and represent it as a matrix. We vary the grid size and compute matrix features for each size. Finally, we represent the entries of a matrix as a column feature vector. The complete feature extraction process is described in Algorithm 1.

---

### Algorithm 1 Computing HOW-Features

---

**Input:** image  $I$  of size  $(w_I, h_I)$ , deformation filtering or Gabor kernels  $\{d_1 \dots d_{N_d}\}$ , grid size set  $\{g_1, \dots, g_{N_g}\}$ .  
**Output:** feature vector  $s$

```

1: for  $i = 1, \dots, N_d$  do
2:   for  $j = 1, \dots, N_g$  do
3:     for  $(w, h) = (1, 1), \dots, (w_I, h_I)$  do
4:        $(x, y) = (\text{TRUNC}(w/g_j), \text{TRUNC}(h/g_j))$  // compute the indices using truncation
5:        $s_{i,j,x,y} = s_{i,j,x,y} + d_i(I(w, h))$  //add the filtered pixel value to the specific bin of the grid
6:     end for
7:   end for
8: end for
9: return  $s$ 

```

---

The HOW-feature has several advantages. It captures the deformation structure that is based on the characteristics of the local shape. Moreover, it uses a local representation that is invariant to local geometric and photometric transformations. This is useful when the translations or rotations are much smaller than the local spatial or orientation grid size.

## V. MANIPULATION USING VISUAL FEEDBACK DICTIONARY

In this section, we present our algorithm used to compute the visual feedback dictionary. At runtime, this dictionary is used to compute the corresponding velocity ( $v$ ) of the controller based on the visual feedback ( $\Delta s(I)$ ).

### A. Building Visual Feedback Dictionary

As shown in figure 2, the inputs of the offline training phase are a set of images and end-effector configurations ( $\{I^{(t)}\}, \{r^{(t)}\}$ ) and the output is the visual feedback dictionary ( $\{\{\Delta s^{(i)}\}, \{v^{(i)}\}\}$ ).

For the training process, the end-effector configurations, ( $\{r^{(t)}\}$ ), are either collected by human tele-operation or generated randomly. A single configuration ( $r^{(i)}$ ) of the robot is a column vector of length  $N_{dof}$ , the number of degrees-of-freedom to be controlled.  $r \in \mathbb{R}^{N_{dof}}$  and its value is represented in the configuration space.

In order to compute the mapping ( $F_H$ ) from the visual feedback to the velocity, we need to transform the configurations  $\{r^{(t)}\}$  and image stream  $\{I^{(t)}\}$  into velocities  $\{v^{(t)}\}$  and the visual feature feedback  $\{\Delta s^{(t)}\}$ . One solution is to select a fixed time step  $\Delta t$  and representing the velocity in

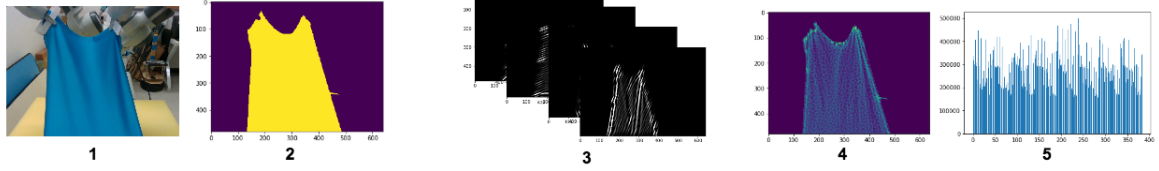


Fig. 4. **Pipeline for HOW-feature Computation:** We use the following stages to the input image (1): (2) Foreground segmentation using Gaussian mixture; (3) Image filtering with multiple orientations and wavelengths of Gabor Kernel; (4) Discretization of the filtered images to form grids of histogram; (5) Stacking the feature matrix to a single column vector.

both the feature and configuration space as:

$$v^{(t)} = \frac{r^{(t+\frac{\Delta t}{2})} - r^{(t-\frac{\Delta t}{2})}}{\Delta t/C_{fr}}; \quad \Delta s(I^{(t)}) = \frac{s(I^{(t+\frac{\Delta t}{2})}) - s(I^{(t-\frac{\Delta t}{2})})}{\Delta t/C_{fr}}$$

where  $C_{fr}$  is the frame rate of the captured video.

However, sampling by a fixed time step ( $\Delta t$ ) leads to a limited number of samples ( $N_I - \Delta t$ ) and can result in over-fitting. To overcome this issue, we break the sequential order of time index to generate more training data from  $I^{(t)}$  and  $r^{(t)}$ . In particular, we assume the manipulation task can be observed as a Markov process [34] and each step is independent from every other. In this case, the sampling rates are given as follows, (when total sampling amount is  $n$ ):

$$v^{(t)} = \frac{r^{(p_t)} - r^{(p_{t+n})}}{(p_t - p_{t+n})/C_{fr}}; \quad \Delta s(I^{(t)}) = \frac{s(I^{(p_t)}) - s(I^{(p_{t+n})})}{(p_t - p_{t+n})/C_{fr}},$$

where  $p_1, \dots, p_n$  is a set of indices randomly generated, and  $p_t \in [1 \dots N_I]$ . In order to build a more concise dictionary, we also apply clustering algorithm such as K-Means Clustering [35] on the feature space. This clustering is used to enhance the performance and prevent the over-fitting problem.

In practice, the visual feedback dictionary can be regarded as an approximation of the interaction function  $F$  (see Equation 1). The overall algorithm to compute the dictionary is given in Algorithm 2.

### B. Sparse Representation

At runtime, we use sparse linear representation [36] to compute the velocity of the controller from the visual feedback dictionary. These representations tend to assign zero



Fig. 5. **Visual Feedback Dictionary:** The visual feedback word is defined by the difference between the visual features  $\Delta s = s - s^*$  and the controller positions  $\Delta r = r - r^*$ . The visual feedback dictionary  $\{\{\Delta s^{(i)}\}, \{\Delta r^{(i)}\}\}$  consists of visual feedback words computed. We show the initial and final states on the left and right, respectively.

weights to most irrelevant or redundant features and are used to find a small subset of most predictive features in the high dimensional feature space. Given a noisy observation of a feature at runtime ( $s$ ) and the visual feedback dictionary constructed by features  $\{s^{(i)}\}$  with labels  $\{l^{(i)}\}$ . We represent  $s$  by  $\hat{s}$ , which is a sparse linear combination of  $\{s^{(i)}\}$ , where  $\beta$  is the sparsity-inducing  $L_1$  term. In order to deal with noisy data, we rather use the  $L_2$  norm on the data-fitting term and formulate the resulting sparse representation as:

$$\hat{\beta} = \arg \min_{\beta} (\|min(s - \sum_i \beta_i s^{(i)})\|_2^2 + \alpha \|\beta\|_1), \quad (6)$$

where  $\alpha$  is a slack variable that is used to balance the trade-off between fitting the data perfectly and using a sparse solution. The sparse coefficient  $\beta^*$  is computed using a minimization formulation:

$$\beta^* = \arg \min_{\beta} (\sum_i \rho(\Delta s_i^* - \sum_j \beta_j \Delta s_i^{(j)}) + \alpha \sum_j \|\beta_j\|_1) \quad (7)$$

After  $\hat{\beta}$  is computed, the observation  $s$  and the probable label  $\hat{l}$  can be reconstructed by the visual feedback dictionary :

$$\hat{s} = \sum_i \hat{\beta}_i s^{(i)} \quad \hat{l} = \sum_i \hat{\beta}_i l^{(i)} \quad (8)$$

The corresponding  $v^*$  of the  $i$ -th DOF in the configuration is given as:

$$v_i^* = \sum_j \beta_j^* v_i^{(j)}, \quad (9)$$

where  $\Delta s_i^{(j)}$  denotes the  $i$ -th data of  $j$ -th feature,  $\Delta s_i^*$  denotes the value of the response, and the norm-1 regularizer  $\sum_j \|\beta_j\|_1$  typically results in a sparse solution in the feature space.

### C. Goal Configuration and Mapping

We compute the goal configuration and the corresponding HOW-features based on the underlying manipulation task at runtime. Based on the configuration, we compute the velocity of the end-effector. The different ways to compute the goal configuration are:

- For the task of manipulating deformable objects to a single state  $m^*$ , the goal configuration can be represented simply by the visual feature of the desired state  $s^* = s(I^*)$ .
- For the task of manipulating deformable objects to a hidden state  $h^*$ , which can be represented by a set

**Algorithm 2** Building the Visual Feedback Dictionary

**Input:** image stream  $\{I^{(t)}\}$  and positions of end-effectors  $\{r^{(t)}\}$  with sampling amount  $n$ , dictionary size  $N_{dic}$

**Output:** Visual Feedback Dictionary  $\{\{\Delta s_d^{(i)}\}, \{\Delta r_d^{(i)}\}\}$

- 1:  $\{\Delta s_d\} = \{\}, \{\Delta r_d\} = \{\}$
- 2:  $p = N_I \text{RAND}(2n)$  // generate random indices for sampling
- 3: **for**  $i = 1, \dots, n$  **do**
- 4:    $\Delta s^{(i)} = s(I^{(p(i))}) - s(I^{(p(i+n))})$  // sampling
- 5:    $\Delta r^{(i)} = r^{(p(i))} - r^{(p(i+n))}$  // sampling
- 6: **end for**
- 7:  $centers = \text{K-MEANS}(\{\Delta s^{(i)}\}, N_{dic})$  // compute the centers of the feature set for clustering
- 8: **for**  $i = 1, \dots, N_{dic}$  **do**
- 9:    $j = \arg \min_i (centers[i] - s^{(i)})$
- 10:    $\{\Delta s_d\} = \{\Delta s_d, \Delta s^{(j)}\}$   $\{\Delta r_d\} = \{\Delta r_d, \Delta r^{(j)}\}$
- 11: **end for**
- 12: **return**  $\{\Delta s_d\}, \{\Delta r_d\}$

of states of the object  $h^* = \{m_1, \dots, m_n\}$  as a set of visual feature  $\{s(I_1), \dots, s(I_n)\}$ . We modify the formulation in Equation 1 to compute  $v$  as:

$$v = -\lambda \min_i (F(s(I) - s(I_j))) \quad (10)$$

- For a complex task, which can be represented using a sequential set of states  $\{m_1, \dots, m_n\}$ , we estimate the sequential cost of each state as  $c(m_i)$ . We use a modification that tends to compute the state with the lowest sequential cost:

$$i^* = \arg \min_i (c(m_i) - \lambda F(s(I) - s(I_i))). \quad (11)$$

After  $i^*$  is computed, the velocity for state  $m_i$  is determined by  $s(I_{i^*})$ , and  $m_i$  is removed from the set of goals for subsequent computations.

1) *Control Parameters Mapping*: The end-effector's configuration  $r$  is represented using the Cartesian coordinates and orientation of the end-effector or the degrees of each joint of the robot. When  $r$  corresponds to the Cartesian coordinates of the end-effectors, an extra step is performed by the inverse kinematics motion planner [37] to map the velocity  $v$  to the actual controlling parameters.

#### D. Human Robot Interaction

In many situations, the robot is working next to the human. The human is either grasping the deformable object or applying forces. We classify the human-robot manipulation task using hidden state goal  $h^*$ , where we need to estimate the human's action repeatedly. As the human intention is unknown to the robot, the resulting deformable material is assigned several goal states  $\{m_1, \dots, m_n\}$ , which are determined conditionally by the action of human.

## VI. IMPLEMENTATION

In this section, we describe our implementation and describe the experimental setup, including the robot and

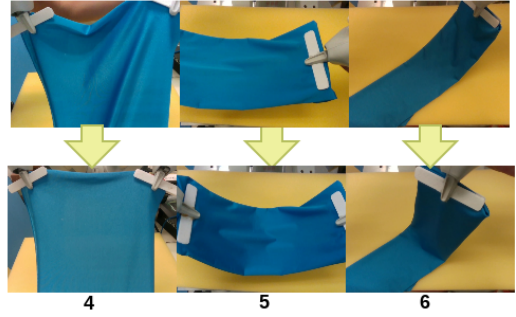


Fig. 6. **Manipulation Benchmarks:** We highlight three benchmarks corresponding to: (4) flattening; (5) placement; (6) folding. Top Row: The initial state of each task. Bottom Row: The goal state of each task. More details are given in Fig. 11.



Fig. 7. **Setup for Manipulation Tasks:** We use a 12-DOF dual-arm ABB YuMi and an RGB camera to perform complex manipulation tasks using visual servoing, with and without humans.

the camera. We also highlight the performance on several manipulation tasks performed by the robot only or robot-human collaboration. We also highlight the benefits of using HOW-features and the visual feedback dictionary.

#### A. Robot Setup

Our algorithm was implemented on a PC and integrated with a ABB YuMi dual-arm robot with 12-DOF to capture  $\{r^{(t)}\}$  and perform manipulation tasks. We use a RealSense camera is used to capture the RGB videos at  $(640 \times 480)$  resolution. In practice, we compute the Cartesian coordinates of the end-effectors of the ABB YuMi as the controlling configuration  $r \in \mathbb{R}^6$  and use an inverse kinematics-based motion planner [37] directly. The setup is shown as Figure 7.

#### B. Benchmarks

To evaluate the effectiveness of our deformable manipulation framework, we use 6 benchmarks with different clothes, having different material characteristics and shapes. Moreover, we use different initial and goal states depending the task, e.g. stretching or folding. In these tasks, we use three different forms of goal configurations for the deformable object manipulations, as discussed in Section V(B). For

benchmarks 4-6, the task corresponds to manipulating the cloth without human participation and we specify the goal configurations. For benchmark 1-3, the task is to manipulate the cloth with human participation. In this the human is assistant with the task, but also introduces external perturbations. Our approach makes no assumption about the human motion, and only uses the visual feedback to guess the human behavior. In benchmark 1, robot needs to anticipate human's pace and forces for grasping to fold the towel in the air. In benchmark 2, robot needs to process a complex task with several goal configurations when performing folding task. In benchmark 3, robot is asked to follow the human's action to maintain the shape of the sheet.

### C. Benefits of HOW-feature

There are many standard techniques known in computer vision and image processing to compute low-dimensional features of deformable models from RGB data. These include standard HOG and color histograms. We evaluated the performance of HOW-features along with the others and also explore combination of these features. The test involved measuring the success rate of the manipulator to move towards the goal configuration based on the computed velocity, as given by Equation 4. We obtain best results in our benchmarks using HOG+HOW features. The HOG features capture the edges in the image and the HOW captures the wrinkles and deformation, so their combination works well.

### D. Visual Feedback Dictionary

The main parameter related to the visual feedback dictionary that govern the performance is its size. At runtime, it is also related to the choice of the slack variable in the sparse representation. As the size of the visual feedback dictionary grows, the velocity error tends to reduce. However, after reaching a certain size, the dictionary contributes less to the control policy mapping. That implies that there is redundancy in the visual feedback dictionary.

### E. Sparse Linear Representation

The performance of sparse representation computation at runtime is governed by the slack variable  $\alpha$  in Equation 6 and 7. This parameter provides a tradeoff between data fitting and sparse solution and governs the velocity error between the desired velocity  $v^*$  and actual velocity,  $\|v - v^*\|_2$ . In practice,  $\alpha$  affects the convergence speed. If  $\alpha$  is small, the sparse computation has little or no impact and the solution tends to a common linear regression. If  $\alpha$  is large, then we suffer from over-fitting.

### F. Comparisons and Benefits

We perform two kinds of experiments to measure the precision of the algorithm on benchmarks 4-6. One is same-subject testing, which separates the same data into two parts. One data is used for training (i.e. dictionary computation) and the other is used for runtime testing. Another kind of experiment is different-subject testing, which uses different data for training and testing. The same-subject testing, which is

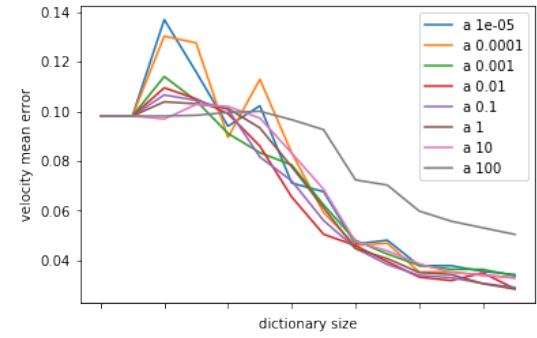


Fig. 8. **Parameter Selection for Visual Feedback Dictionary and Sparse Representation:** We vary the dictionary size on the X-axis and compute the velocity error for different values of  $\alpha$  chosen for sparse representation for benchmark 1.

similar to online learning method, shows faster convergence with a smaller dictionary size. The different-subject testing highlights that our visual feedback dictionary computation algorithm can be used for different environments. We highlight their performance in terms of regression results in Figure 9. We notice that the errors are comparable.

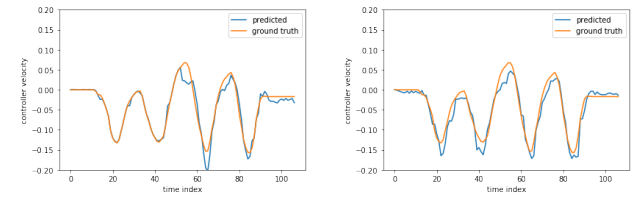


Fig. 9. **Regression Result for Different Training methods:** The fitted and original data in terms of computing the controller's velocity is shown: (a) Regression model trained same-subject data; (b) Regression model trained using different-subject data.

## VII. CONCLUSION, LIMITATIONS AND FUTURE WORK

We present an approach to manipulate deformable materials using visual servoing and a precomputed feedback dictionary. We present a new algorithm to compute HOW-features, which capture the shape variation and local features of the deformable material. The visual feedback dictionary is precomputed using sampling and clustering techniques and used with sparse representation to compute the velocity of the controller to perform the task. We highlight the performance on a 12-DOF ABB dual arm and perform complex tasks related to stretching, folding, and placement. Furthermore, our approach can also be used for human-robot collaborative tasks.

Our approach has some limitations. We make some assumptions about the deformable material and the movements of the end-effector. The effectiveness of the manipulation algorithm is governed by the offline training data and the sparse representation. The accuracy of HOW-feature computations can also vary based on the illumination and relative colors of the cloth. There are many avenues for future work. Besides overcoming these limitations, we would like our approach for more complex tasks such as human

Feature	Benchmark4	Benchmark5	Benchmark6
HOG	71.44%	67.31%	82.62%
Color Histograms	62.87%	53.67%	97.04%
HOW	92.21%	71.97%	85.57%
HOW+HOG	94.53%	84.08%	95.08%

Fig. 10. **Comparison between Deformable Features:** We compared the performance of four deformable features HOG, Color Histograms, HOW and HOW+HOG on three benchmarks. We evaluated the success rate of the manipulator in terms of reaching the goal configuration based on the velocity computed using those features. Overall, we obtain the best performance by using HOG + HOW features.

Benchmark #	Object	Initial State	Task/Goal
1	towel	unfold in the air	fold with human
2	shirt	shape (set by human)	fixed shape
3	unstretchable cloth	position (set by human)	fixed shape
4	stretchable cloth	random	flattening
5	stretchable cloth	random	placement
6	stretchable cloth	unfolded shape on desk	folded shape

Fig. 11. **Benchmark Tasks:** We highlight various complex manipulation tasks performed using our algorithm. Three of them involve human-robot collaboration and we demonstrate that our method can handle external forces and perturbations applied to the cloth. We use cloth benchmarks of different material characteristics. The initial state is a random configuration or an unfolded cloth on a table, and we specify the final configuration for the task. The benchmark # correspond to the numbers shown in Fig. 1 and Fig. 8

dressing. Furthermore, we could use deep learning methods to compute the control policy mapping.

## REFERENCES

- [1] S. Miller, J. van den Berg, M. Fritz, T. Darrell, K. Goldberg, and P. Abbeel, “A geometric approach to robotic laundry folding,” *The International Journal of Robotics Research*, vol. 31, no. 2, pp. 249–267, 2011.
- [2] A. Kapusta, W. Yu, T. Bhattacharjee, C. K. Liu, G. Turk, and C. C. Kemp, “Data-driven haptic perception for robot-assisted dressing,” in *IEEE International Symposium on Robot and Human Interactive Communication*, 2016, pp. 451–458.
- [3] Y. Gao, H. J. Chang, and Y. Demiris, “Iterative path optimisation for personalised dressing assistance using vision and force information,” in *IEEE/RSJ International Conference on Intelligent Robots and Systems*, 2016, pp. 4398–4403.
- [4] Y. Li, X. Hu, D. Xu, Y. Yue, E. Grinspun, and P. K. Allen, “Multi-sensor surface analysis for robotic ironing,” in *IEEE International Conference on Robotics and Automation*, 2016, pp. 5670–5676.
- [5] L. Twardon and H. Ritter, “Interaction skills for a coat-check robot: Identifying and handling the boundary components of clothes,” in *IEEE International Conference on Robotics and Automation*, 2015, pp. 3682–3688.
- [6] J. Schrimpf, L. E. Wetterwald, and M. Lind, “Real-time system integration in a multi-robot sewing cell,” in *IEEE/RSJ International Conference on Intelligent Robots and Systems*, 2012, pp. 2724–2729.
- [7] D. Kruse, R. J. Radke, and J. T. Wen, “Collaborative human-robot manipulation of highly deformable materials,” in *IEEE International Conference on Robotics and Automation*, 2015, pp. 3782–3787.
- [8] L. Bodenhagen, A. R. Fugl, A. Jordt, M. Willatzen, K. A. Andersen, M. M. Olsen, R. Koch, H. G. Petersen, and N. Krüger, “An adaptable robot vision system performing manipulation actions with flexible objects,” *IEEE transactions on automation science and engineering*, vol. 11, no. 3, pp. 749–765, 2014.
- [9] D. Berenson, “Manipulation of deformable objects without modeling and simulating deformation,” in *Intelligent Robots and Systems (IROS), 2013 IEEE/RSJ International Conference on*. IEEE, 2013, pp. 4525–4532.
- [10] D. Navarro-Alarcon, Y. H. Liu, J. G. Romero, and P. Li, “Model-free visually servoed deformation control of elastic objects by robot manipulators,” *IEEE Transactions on Robotics*, vol. 29, no. 6, pp. 1457–1468, 2013.
- [11] D. Navarro-Alarcon, H. M. Yip, Z. Wang, Y. H. Liu, F. Zhong, T. Zhang, and P. Li, “Automatic 3-d manipulation of soft objects by robotic arms with an adaptive deformation model,” *IEEE Transactions on Robotics*, vol. 32, no. 2, pp. 429–441, 2016.
- [12] D. Kruse, R. J. Radke, and J. T. Wen, “Collaborative human-robot manipulation of highly deformable materials,” in *IEEE International Conference on Robotics and Automation*, 2015, pp. 3782–3787.
- [13] M. J. Sullivan and N. P. Papanikolopoulos, “Using active-deformable models to track deformable objects in robotic visual servoing experiments,” in *IEEE International Conference on Robotics and Automation*, vol. 4, 1996, pp. 2929–2934.
- [14] A. Ramisa, G. Alenyà, F. Moreno-Noguer, and C. Torras, “Using depth and appearance features for informed robot grasping of highly wrinkled clothes,” in *Robotics and Automation (ICRA), 2012 IEEE International Conference on*. IEEE, 2012, pp. 1703–1708.
- [15] Y. Li, C.-F. Chen, and P. K. Allen, “Recognition of deformable object category and pose,” in *IEEE International Conference on Robotics and Automation*, 2014, pp. 5558–5564.
- [16] C. Bersch, B. Pitzer, and S. Kammel, “Bimanual robotic cloth manipulation for laundry folding,” in *IEEE/RSJ International Conference on Intelligent Robots and Systems*, 2011, pp. 1413–1419.
- [17] A. Clegg, W. Yu, Z. Erickson, C. K. Liu, and G. Turk, “Learning to navigate cloth using haptics,” *arXiv preprint arXiv:1703.06905*, 2017.
- [18] Y. Bai, W. Yu, and C. K. Liu, “Dexterous manipulation of cloth,” in *Computer Graphics Forum*, vol. 35, no. 2, 2016, pp. 523–532.
- [19] P.-C. Yang, K. Sasaki, K. Suzuki, K. Kase, S. Sugano, and T. Ogata, “Repeatable folding task by humanoid robot worker using deep learning,” *IEEE Robotics and Automation Letters*, vol. 2, no. 2, pp. 397–403, 2017.
- [20] M. Cusumano-Towner, A. Singh, S. Miller, J. F. O’Brien, and P. Abbeel, “Bringing clothing into desired configurations with limited perception,” in *IEEE International Conference on Robotics and Automation*, 2011, pp. 3893–3900.
- [21] F. Chaumette and S. Hutchinson, “Visual servo control. i. basic approaches,” *IEEE Robotics & Automation Magazine*, vol. 13, no. 4, pp. 82–90, 2006.
- [22] S. Hutchinson, G. D. Hager, and P. I. Corke, “A tutorial on visual servo control,” *IEEE transactions on robotics and automation*, vol. 12, no. 5, pp. 651–670, 1996.
- [23] Q. Bateux and E. Marchand, “Histograms-based visual servoing,” *IEEE Robotics and Automation Letters*, vol. 2, no. 1, pp. 80–87, 2017.
- [24] S. Hirai and T. Wada, “Indirect simultaneous positioning of deformable objects with multi-pinchng fingers based on an uncertain model,” *Robotica*, vol. 18, no. 1, pp. 3–11, 2000.
- [25] J. D. Langsfeld, A. M. Kabir, K. N. Kaipa, and S. K. Gupta, “Online learning of part deformation models in robotic cleaning of compliant objects,” in *ASME Manufacturing Science and Engineering Conference*, vol. 2, 2016.
- [26] J. Van Den Berg, S. Miller, K. Goldberg, and P. Abbeel, “Gravity-based robotic cloth folding,” in *Algorithmic Foundations of Robotics IX*. Springer, 2010, pp. 409–424.
- [27] C. Collewet and E. Marchand, “Photometric visual servoing,” *IEEE Transactions on Robotics*, vol. 27, no. 4, pp. 828–834, 2011.
- [28] Q. Bateux and E. Marchand, “Direct visual servoing based on multiple intensity histograms,” in *IEEE International Conference on Robotics and Automation*, 2015, pp. 6019–6024.
- [29] D.-S. Lee, “Effective gaussian mixture learning for video background subtraction,” *IEEE transactions on pattern analysis and machine intelligence*, vol. 27, no. 5, pp. 827–832, 2005.
- [30] T. S. Lee, “Image representation using 2d gabor wavelets,” *IEEE Transactions on pattern analysis and machine intelligence*, vol. 18, no. 10, pp. 959–971, 1996.
- [31] J. G. Daugman, “Uncertainty relation for resolution in space, spatial frequency, and orientation optimized by two-dimensional visual cortical filters,” *JOSA A*, vol. 2, no. 7, pp. 1160–1169, 1985.
- [32] K. Yamazaki and M. Inaba, “A cloth detection method based on image wrinkle feature for daily assistive robots,” in *IAPR Conference on Machine Vision Applications*, 2009, pp. 366–369.
- [33] N. Dalal and B. Triggs, “Histograms of oriented gradients for human detection,” in *IEEE Conference on Computer Vision and Pattern Recognition*, vol. 1, 2005, pp. 886–893.
- [34] L. E. Baum, “An inequality and associated maximization technique in statistical estimation for probabilistic functions of markov process,” *Inequalities*, vol. 3, pp. 1–8, 1972.

- [35] J. A. Hartigan and M. A. Wong, "Algorithm as 136: A k-means clustering algorithm," *Journal of the Royal Statistical Society. Series C (Applied Statistics)*, vol. 28, no. 1, pp. 100–108, 1979.
- [36] D. L. Donoho and M. Elad, "Optimally sparse representation in general (nonorthogonal) dictionaries via 1 minimization," *Proceedings of the National Academy of Sciences*, vol. 100, no. 5, pp. 2197–2202, 2003.
- [37] P. Beeson and B. Ames, "Trac-ik: An open-source library for improved solving of generic inverse kinematics," in *IEEE-RAS 15th International Conference on Humanoid Robots*, 2015, pp. 928–935.